Quantitative phosphoproteomic analysis reveals vasopressin V2-receptor–dependent signaling pathways in renal collecting duct cells

Markus M. Rinschen[a,b], Ming-Jiun Yu[a], Guanghui Wang[c], Emily S. Boja[c], Jason D. Hoffert[a], Trairak Pisitkun[a], and Mark A. Knepper[a,1]

[a]Epithelial Systems Biology Laboratory, National Heart, Lung and Blood Institute, National Institutes of Health, Bethesda, MD 20892; [b]Department of Internal Medicine D, University of Muenster, Muenster, Germany; and [c]Proteomics Core Facility, National Heart, Lung and Blood Institute, National Institutes of Health, Bethesda, MD 20892

Edited* by Peter Agre, Johns Hopkins Malaria Research Institute, Baltimore, MD, and approved December 22, 2009 (received for review September 16, 2009)

Vasopressin's action in renal cells to regulate water transport depends on protein phosphorylation. Here we used mass spectrometry–based quantitative phosphoproteomics to identify signaling pathways involved in the short-term V2-receptor–mediated response in cultured collecting duct cells (mpkCCD) from mouse. Using Stable Isotope Labeling by Amino acids in Cell culture (SILAC) with two treatment groups (0.1 nM dDAVP or vehicle for 30 min), we carried out quantification of 2884 phosphopeptides. The majority (82%) of quantified phosphopeptides did not change in abundance in response to dDAVP. Analysis of the 273 phosphopeptides increased by dDAVP showed a predominance of so-called "basophilic" motifs consistent with activation of kinases of the AGC family. Increases in phosphorylation of several known protein kinase A targets were found. In addition, increased phosphorylation of targets of the calmodulin-dependent kinase family was seen, including autophosphorylation of calmodulin-dependent kinase 2 at T286. Analysis of the 254 phosphopeptides decreased in abundance by dDAVP showed a predominance of so-called "proline-directed" motifs, consistent with down-regulation of mitogen-activated or cyclin-dependent kinases. dDAVP decreased phosphorylation of both JNK1/2 (T183/Y185) and ERK1/2 (T183/Y185; T203/Y205), consistent with a decrease in activation of these proline-directed kinases in response to dDAVP. Both ERK and JNK were able to phosphorylate residue S261of aquaporin-2 in vitro, a site showing a decrease in phosphorylation in response to dDAVP in vivo. The data support roles for multiple vasopressin V2-receptor–dependent signaling pathways in the vasopressin signaling network of collecting duct cells, involving several kinases not generally accepted to regulate collecting duct function.

aquaporin-2 | MAP kinase | mass spectrometry | protein kinase A | SILAC

Regulation of osmotic water transport across the renal collecting duct epithelium is responsible for precise control of renal water excretion and regulation of the osmolality of body fluids. This precise control is achieved largely by actions of the peptide hormone vasopressin to regulate the water channel aquaporin-2 (AQP2) in collecting duct cells. Vasopressin binds to a G protein–coupled receptor (the type 2 vasopressin receptor or V2R) in the basolateral plasma membrane of collecting duct (CD) principal cells, triggering a complex signaling response that involves an increase in intracellular cAMP and spike-like, aperiodic increases in intracellular calcium (1, 2).

The advent of methodologies for large-scale, mass spectrometry (MS)–based phosphoproteomics offers the opportunity for comprehensive discovery of signaling pathways in mammalian cells. In particular, the Stable Isotope Labeling by Amino acids in Cell culture (SILAC) methodology is a metabolic-labeling approach that allows high-precision quantification of individual peptides in cultured cells using tandem MS (3), leading to powerful quantitative approaches to discovery of signaling pathways (4–6). Recently, we generated a subclone of the mpkCCD mouse collecting duct cell line (designated "clone 11 mpkCCD cells") that exhibits high levels of AQP2 expression, V2R-mediated trafficking of AQP2 to the apical plasma membrane, and V2R-mediated AQP2 phosphorylation resembling that seen in native collecting duct cells (7). Here we apply the SILAC method to analysis of the phosphoproteomic response of clone 11 mpkCCD cells to the short-term action of the V_2R-selective vasopressin analog dDAVP.

Results

Technical Controls. Incorporation of labeled amino acids was found to be 98% complete after 16 days of growth of mpkCCD cells (Table S1), providing a standard for further experimentation. Transepithelial resistance was not statistically different between cells labeled with heavy versus light amino acids, either before or after addition of the vasopressin analog dDAVP (Fig. S1*A*). As described previously (7), phosphorylation of S261was decreased within 30 min of dDAVP treatment (0.1 nM), whereas phosphorylation at S269 was increased (Fig. S1*B*), confirming responsivity of the mpkCCD cells to the vasopressin analog.

Phosphoproteomic Profiling and Quantification. In total, 35,585 peptide scans passed target-decoy criteria (false discovery rate <2% for single peptides). Analysis of datasets using three search algorithms (SEQUEST, InsPecT, and OMSSA) revealed 3,869 unique phosphopeptides (4,136 phosphorylation sites) corresponding to 1,695 phosphoproteins (Datasets S1). (These data can be accessed at http://dir.nhlbi.nih.gov/papers/lkem/cdpd_private/.) Approximately 45% of the reported phosphorylation sites have not been previously identified in the mouse phosphoproteome according to the Phosphosite database (www.phosphosite.org). Twenty three percent (949 phosphorylation sites) appear to be present in the known human phosphoproteome, based on mapping of mouse phosphopeptides to data in the Human Protein Reference Database (http://www.hprd.org/). Each of the three search algorithms added a significant number of identifications (Fig. 1*A*). A total of 3,435 peptides were identified by MS2 spectra, whereas 434 were identified only by MS3 spectra (Fig. 1*B*).

The areas under the MS1–time-course curves for heavy and light forms of 2,884 unambiguous peptides were quantified. Figure 1*C* shows a histogram of all quantified phosphopeptide ratios measured in at least one of the three experiments, showing that the majority did not change substantially. The dashed lines in Fig. 1*C* show the 95% confidence interval defined on the basis

Author contributions: M.M.R., M.-J.Y., J.D.H., T.P., and M.A.K. designed research; M.M.R. and G.W. performed research; G.W., E.S.B., J.D.H., T.P., and M.A.K. contributed new reagents/analytic tools; M.M.R., M.-J.Y., J.D.H., T.P., and M.A.K. analyzed data; and M. M.R., M.-J.Y., J.D.H., and M.A.K. wrote the paper.

The authors declare no conflict of interest.

*This Direct Submission article had a prearranged editor.

[1]To whom correspondence should be addressed. E-mail: knep@helix.nih.gov.

This article contains supporting information online at www.pnas.org/cgi/content/full/0910646107/DCSupplemental.

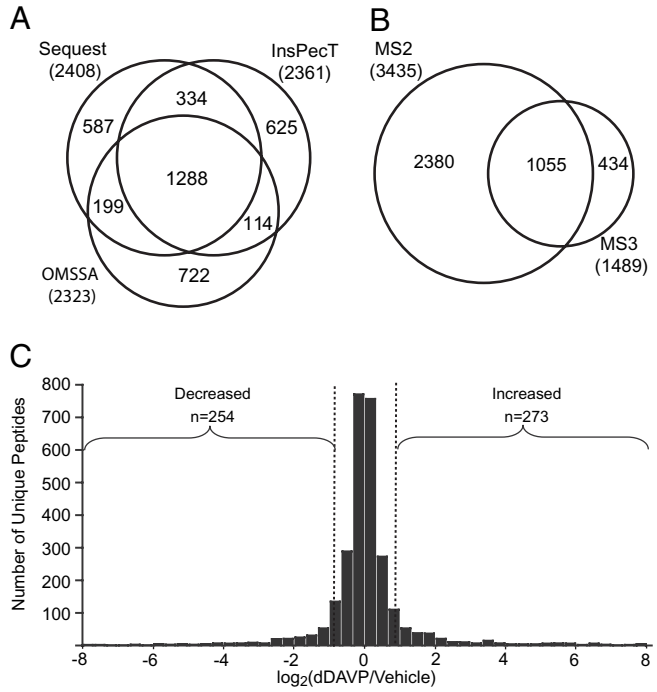

Fig. 1. Phosphopeptides identified in mpkCCD cells. (*A*) Venn diagram of phosphopeptides identified by three search algorithms (SEQUEST, InsPecT, and OMSSA). Numbers are unique peptides identified. (*B*) Phosphopeptides identified in MS2 and MS3 scans. (*C*) Distribution of changes for all quantified phosphopeptides. Dashed lines show 95% confidence interval with no experimental perturbation (defined on the basis of preliminary experiments in which both samples were vehicle treated). Brackets indicate phosphopeptides decreased or increased.

of preliminary experiments in which both samples were vehicle treated (Tables S1). Based on this criterion, 273 of the phosphopeptide abundances were increased and 254 were decreased in response to dDAVP. The sequences surrounding the phosphorylated amino acid residues for the regulated peptides were further analyzed to classify the kinases that may be involved. First, we carried out motif analysis using *motif-x* (8) (Fig. 2 *A* and *B*). The *motif-x* algorithm generates position-weighted matrices representing amino acid sequences that are significantly overrepresented in the input data sets. Among the 273 peptides in the "increased" group, three basophilic motifs with an arginine residue at −3 were overrepresented (Fig. 2*A*). Among the 254 peptides in the "decreased" group, three proline-directed motifs (P at +1) were found to be enriched (Fig. 2*B*). These motif assignments were not affected by use of more stringent thresholds (Fig. S2*A*). A second way to classify phosphorylation motifs is a binary decision tree (*Methods*) (9). Figure 2 *C* and *D* show the frequency of basophilic, proline-directed, and acidophilic sites. The up-regulated phosphorylation sites in each experiment are dominated by basophilic motifs (Fig. 2*C*), confirming findings shown in Fig. 2*A*. In contrast, the down-regulated sites are dominated by proline-directed motifs (Fig. 2*D*). It should be noted that 95% of phosphorylation sites identified were on serines or threonines. A list of tyrosine phosphopeptides that were up-regulated or down-regulated in response to dDAVP is given in Dataset S2. Tables 1 and 2 list individual proteins with regulated phosphorylation sites that were found in all three experimental sample pairs. We extracted Gene Ontology (GO) terms from the combined list of regulated phosphoproteins (Tables 1 and 2) to assess what processes might be regulated by the phosphorylation changes observed. Particularly prominent are proteins with GO *component* terms "plasma membrane" (*Aak1, Ctnnb1, Ctnnd1, Cxadr, Fnbp1l, Ppl, Tjp1, Tjp3*) and "cytoskeleton" (*Ctnnb1, Epb4.1l1, Fnbp1l, Marcks, Pdlim2, Plec1, Ppl, Ubr4),* proteins with GO *processes* of "transcriptional regulation" (*Csda, Ctnnb1, Ctnnd1, Mcm2*), "cell adhesion" (*Ctnnb1, Ctnnd1, Cxadr*), or "protein amino acid phosphorylation" (*Aak1, Map4k5, Pctk3*). In addition, there were several proteins that contained PDZ domains (*Ahnak, Pdlim2, Slc9a3r1, Tjp1, Tjp3*) that could be involved in apical–basolateral polarity determination (10) and AQP2 trafficking (11).

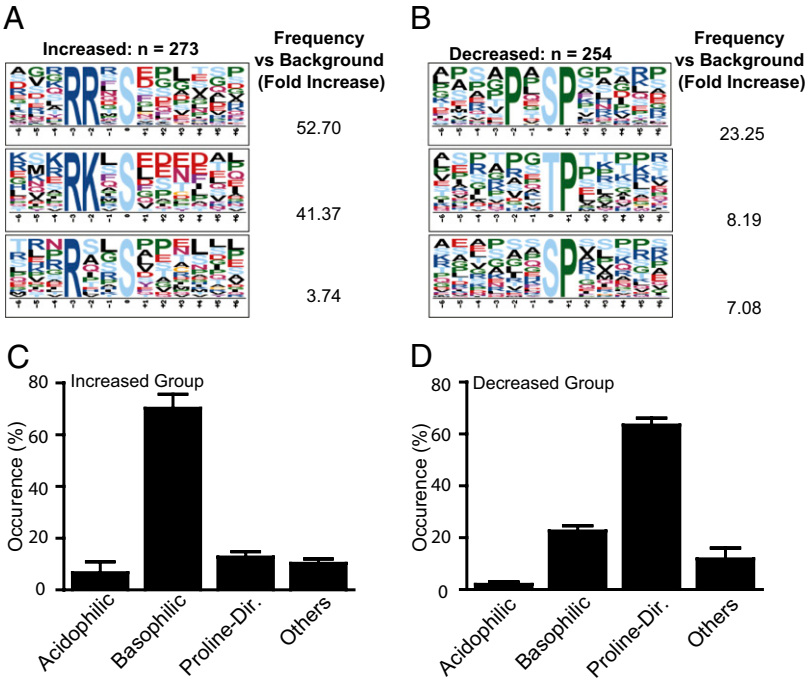

Fig. 2. (*A*) Sequence logos showing overrepresented phosphorylation motifs in 273 phosphopeptides increased by dDAVP. Position 0 represents phosphorylated residue. Basophilic phosphorylation motifs dominate up-regulated peptide population. (*B*) Sequence logos showing overrepresented phosphorylation motifs in 254 phosphopeptides down-regulated by dDAVP. Proline-directed motifs are most common. (*C*) Phosphorylation motifs for dDAVP–up-regulated phosphopeptides determined by binary decision tree–based method. Error bars indicate SEM. (*D*) Phosphorylation motifs for dDAVP–down-regulated phosphopeptides based on binary decision tree-based method.

Table 1. Phosphopeptides quantified in all three experiments and decreased in abundance in response to dDAVP

Peptide sequence	RefSeq	Gene symbol	Protein name	Site	$\log_2$ (dDAVP/vehicle) (mean ± SE)
RLPSSPASPS*PK	NP_001003815	*Epb4.1l1*	Erythrocyte protein band 4.1-like 1 isoform b	S533	−3.57 ± 0.54
RLPSSPAS*PSPK	NP_001003815	*Epb4.1l1*	Erythrocyte protein band 4.1-like 1 isoform b	S531	−2.42 ± 0.22
EQTAS*APAT*PLVSK	NP_081501	*Cobll1*	Cobl-like 1 isoform 2	S268, T272	−2.35 ± 0.47
GKYS*PTVQTR	NP_032935	*Ppl*	Periplakin	S14	−2.24 ± 0.51
AEDGAAPSPSSET*PK	NP_032564	*Marcks*	Myristoylated alanine rich protein kinase C substrate	T143	−2.2 ± 0.28
APLLSEPASAVPTS*PFR	NP_001074646	*Kif13b*	Kinesin family member 13B	S1654	−2.19 ± 0.33
EQTAS*APATPLVSK	NP_081501	*Cobll1*	Cobl-like 1 isoform 2	S268	−2.06 ± 0.47
TASRPEDTPDSPSGPSS*PK	NP_081101	*Lrrc16a*	Leucine-rich repeat containing 16A	S1295	−2.01 ± 0.22
EALVEPASES*PRPALAR	NP_036160	*Slc9a3r1*	Solute carrier family 9, isoform 3 regulator 1 ("NHERF1")	S275	−1.82 ± 0.03
APQS*PTLAPAK	NP_001020363	*Cxadr*	Coxsackievirus and adenovirus receptor isoform a	S332	−1.64 ± 0.27
IDS*PGLKPASQQK	NP_033412	*Tjp1*	Tight junction protein 1 isoform 1 ("ZO-1")	S912	−1.43 ± 0.13
HGS*DPAFGPSPR	NP_598848	*Fam83h*	Family with sequence similarity 83, member H	S522	−0.88 ± 0.17
ALT*PSIEAK	NP_033151	*Atxn2*	Ataxin 2	T710	−0.82 ± 0.15
ANESS*PKPAGPPPER	NP_660126	*Aif1l*	Allograft Inflammatory factor 1-like	S134	−0.76 ± 0.11
GGVTGS*PEASISGSK	NP_033773	*Ahnak*	AHNAK nucleoprotein isoform 1	S5504	−0.73 ± 0.13
SLS*PIIGK	NP_001003815	*Epb4.1l1*	Erythrocyte protein band 4.1-like 1 isoform b	S769	−0.7 ± 0.15
GACST*PEMPQFESVK	NP_001003815	*Epb4.1l1*	Erythrocyte protein band 4.1-like 1 isoform b	T672	−0.66 ± 0.02
STS*VDDTDKSSSEAIMVR	NP_081501	*Cobll1*	Cobl-like 1 isoform 2	S334	−0.49 ± 0.1
VLLHS*PGRPS*SPR	NP_666090	*Pdlim2*	PDZ and LIM domain 2	S199, S204	−0.47 ± 0.1
AIAEPES*PGESR	NP_038797	*Tjp3*	Tight junction protein 3	S343	−0.44 ± 0.05
VGSLT*PPSS*PK	NP_001035195	*Aak1*	AP2 associated kinase 1 isoform 1	T618, S622	−0.43 ± 0.08
VLLHS*PGRPSS*PR	NP_666090	*Pdlim2*	PDZ and LIM domain 2	S199, S205	−0.43 ± 0.04
TIS*DGTISAAK	NP_001108137	*Fnbp1l*	Formin binding protein 1-like isoform 1	S295	−0.31 ± 0.06
NSSS*PVSPASVPGQR	NP_665835	*Eap1*	Enhanced at puberty protein 1	S638	−0.31 ± 0.07
S*GDLGDMEPLK	NP_001078917	*Ctnnd1*	Catenin, delta 1 isoform 2	S899	−0.27 ± 0.06
LGASNS*PGQPNSVK	NP_081625	*Rbm25*	RNA binding motif protein 25	S672	−0.18 ± 0.03
MDRT*PPPPTLS*PAAVTVGR	NP_700470	*Phc3*	Polyhomeotic-like 3	T607, S614	−0.11 ± 0.02

Confirmation of SILAC Quantification. To confirm selected quantifications from MS, immunoblotting was carried out using commercially available phosphospecific antibodies against 18 detected phosphorylation sites. Changes in protein phosphorylation observed by immunoblotting showed a significant correlation with the mean changes based on MS quantification ($P < 0.001$; Fig. 3). Examples of these immunoblots are shown in Fig. S2*B*. A significant increase in phosphorylation was confirmed in β-catenin (*Ctnnb1*) at S552, BCL2-associated agonist of cell death (*Bad*) at S112 and S136, yes-associated protein 1 (*Yap1*) at S112; eukaryotic translation initiation factor 4E binding protein 1 (*Eif4ebp1*) at T69 and stathmin (*Stmn*) at S15. A significant decrease in phosphorylation was found for N-myc downstream regulated gene (*Ndrg1*) at S330, and lamin A/C (*Lmna*) at S22.

AQP2 phosphorylation sites were not included in this analysis because of the presence of four closely spaced phosphorylated serines in the COOH-terminal tail, giving MS-quantified peptides with multiple phosphorylation sites. Examples of quantification of these AQP2 peptides are shown in Fig. S3*A*.

Confirmation of Data-Dependent SILAC Quantification by Targeted Ion Selection. For protein targets for which phosphospecific antibodies were unavailable, we used MS-based targeted ion selection (TIS) to analyze for confirmation. With this, we confirmed the "data-dependent" quantification of 46 additional peptides (Table S3). The correlation between the ratios from the data-dependent experiment and the TIS experiment was highly significant ($P < 0.001$; Fig. S5*B*).

Role of Basophilic Kinases in Vasopressin Signaling. The general increase in phosphorylation at basophilic sites (Fig. 2 *A* and *C*) in response to short-term dDAVP is consistent with the well-established role for protein kinase A (PKA) in CD cells (12). Several known PKA phosphorylation sites increased in response to dDAVP in our study, including *Ctnnb1* at S552; *Bad* at S112, S136 and S155 (Fig. 3), *Canx* at S582 (Table 2), as well as *Arhgef7* at S673, *DNAjc5* at S8, *Flna* at S2144, *Itpr3* at S1832, *Nedd4l* at S449, *Pde4d* at S129, *Pfkfb2* at S447, and *Rps6* at S236/240 (Table S2). A second family of basophilic kinases is the Ca^{2+}-calmodulin (CaM)–dependent kinases. Previous studies have demonstrated that vasopressin increases intracellular calcium and results in a CaM-dependent increase in myosin regulatory light chain phosphorylation in the inner medullary collecting duct (13). To address further the role of CaM-dependent kinases, we immunoblotted for the activating autophosphorylation site of CaM-dependent kinase II (CaMK II) (T286) (14). Phosphorylation at this site increased in both mpkCCD cells (Fig. S4*A*) and native rat inner medullary collecting duct (Fig. S4*B*) following dDAVP. Phosphorylation of S15 of stathmin, a protein phosphorylation believed to be medi-

Table 2. Phosphopeptides quantified in all three experiments and increased in abundance in response to dDAVP

Peptide sequence	RefSeq	Gene symbol	Protein name	Site	$\log_2$ (dDAVP/vehicle) (mean ± SE)
LRT*DAPEELIEKIR	NP_083151	*Xrcc3*	X-ray repair complementing defective repair in Chinese hamster cells 3	T163	5.45 ± 0.77
RIS*DPLTSSPGR	NP_032590	*Mcm2*	Minichromosome maintenance deficient 2 mitotin	S21	2.76 ± 0.52
VNT*YPEDSLPDEEK	NP_958927	*Map4k5*	Mitogen-activated protein kinase kinase kinase kinase 5	T400	1.92 ± 0.16
SS*FSNSADDIK	NP_001070257	*Cbx5*	Chromobox homolog 5	S93	1.92 ± 0.44
S*CDLAGVETCK	NP_079580	*Lcmt1*	Leucine carboxyl methyltransferase 1	S247	1.89 ± 0.27
KSS*FSNSADDIK	NP_001070257	*Cbx5*	Chromobox homolog 5	S93	1.88 ± 0.42
S*RPLNAVSQDGK	NP_035863	*Csda*	Cold shock domain protein A short isoform	S259	1.86 ± 0.42
TS*MGGTQQQFVEGVR	NP_031640	*Ctnnb1*	Catenin (cadherin associated protein), beta 1	S552	1.58 ± 0.03
RFS*MEDLNK	NP_032821	*Pctk3*	PCTAIRE protein kinase 3	S66	0.84 ± 0.16
RSS*SELSPEVVEK	NP_780438	*Srrm2*	Serine/arginine repetitive matrix 2	S1243	0.82 ± 0.19
RGS*FSSENYWR	NP_766531	*Alkbh5*	alkB, Alkylation repair homolog 5	S362	0.69 ± 0.15
AEEDEILNRS*PR	NP_001103969	*Canx*	Calnexin	S582	0.65 ± 0.23
RGS*LTFAGESSK	NP_598848	*Fam83h*	Family with sequence similarity 83, member H	S970	0.58 ± 0.04
S*SSVGSSSSYPISSAGPR	NP_001157012	*Plec1*	Plectin 1 isoform 12alpha	S4391	0.34 ± 0.01
EEVAS*EPEEAASPTTPK	NP_077155	*Nop56*	Nucleolar protein 5A	S536	0.27 ± 0.02
HVTLPSS*PR†	NP_001153791	*Ubr4*	Retinoblastoma-associated factor 600	S2716	0.25 ± 0.03
HVTLPS*SPR†	NP_001153791	*Ubr4*	Retinoblastoma-associated factor 600	S2715	0.24 ± 0.03

†Ambiguous phosphorylation site assignment on manual spectra examination.

ated by Ca/CaM-dependent kinases (15), was increased (Dataset S1 and Fig. 3).

We also examined phosphorylation of two transcription factors that are typically phosphorylated by basophilic kinases, namely Creb1 and FoxO1 (Fig. S5*C*). Creb1 phosphorylation at S133 was increased, as previously shown (16), but there was no change in phosphorylation of FoxO1. Creb1 is activated by phosphorylation at S133 by different basophilic kinases, namely Ca/CaM-dependent kinases, ribosomal S6 kinases, and protein kinase A (17).

Role of Proline-Directed Kinases in Vasopressin Signaling. The abundance of down-regulated, proline-directed phosphorylation sites in response to dDAVP points to MAP kinases or cyclin-dependent kinases as likely candidates for mediators of the phosphorylation events (18). Because of the dominance of the position weighted matrix showing a proline both at −2 and +1, we suspected a role for MAP kinases. Hence, immunoblotting was carried out for regulatory phosphorylation sites in ERK1/2 (*Mapk3, Mapk1*), JNK1/2 (*Mapk8, Mapk9*), and p38-kinase α (*Mapk14*) (Fig. 4 *A* and Fig. S5*A*). Phosphorylated ERK and JNK were decreased, but not p38α. The immunoblot data for phosphorylated ERK (decreased) and p38α (unchanged) are in accordance with MS results (Fig. 2).

MAP kinases are typically involved in regulation of gene expression and differentiation. JNK has been shown to phosphorylate the CREB family transcription factor ATF2 as well as c-Jun and c-Myc at regulatory proline-directed sites [reviewed in (19)]. A decrease in phosphorylation was found for c-Jun (S73) and ATF2 (T51/53) (Fig. 4*B* and Fig. S5*B*).

The combination of decreased activation of ERK and JNK, and a general decrease of proline-directed sites provides a potential explanation for the decreased phosphorylation of AQP2 at S261 (^{260}H-^{261}S-^{262}P) in response to vasopressin (Fig. S1*B*). Incubations of synthetic AQP2 COOH-terminal peptides with several candidate kinases (Fig. 5) revealed that JNK, p38, CDK1, and CDK5 can all phosphorylate the AQP2 peptide at S261. ERK1 weakly phosphorylated the site.

Discussion

Vasopressin is the key hormone in the renal regulation of water excretion. Comprehensive knowledge of its mechanism of action is needed to understand and treat water balance disorders such as

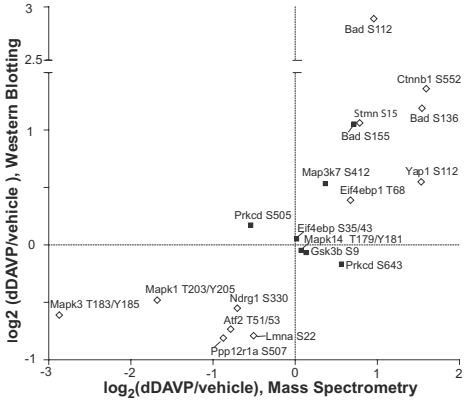

Fig. 3. Quantification of phosphorylation changes in response to dDAVP for selected proteins: SILAC-based MS vs. immunoblotting with phosphospecific antibodies. Correlation is statistically significant ($P < 0.001$, $R^2 = 0.44$). Open squares indicate significant changes by immunoblotting ($P < 0.05$, *t* test).

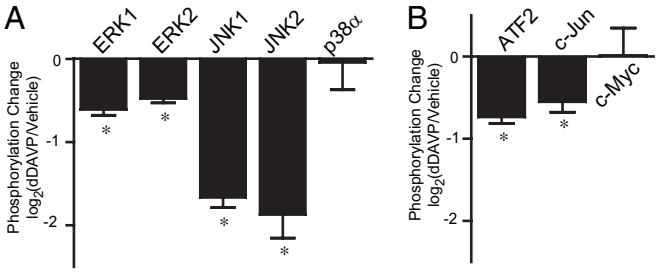

Fig. 4. (*A*) Changes in phosphorylation at regulatory sites of MAP kinases, response to dDAVP. Data are from immunoblotting with phospho-specific antibodies (examples of primary data, Fig. S5*A*): ERK1, pT203/Y205; ERK2, pT183/Y185; JNK 1/2, pT183/Y185; p38α pT179/Y181. Mean ± SE ($n = 6$ pairs). Asterisks indicate statistical significance ($P < 0.05$). (*B*) Immunoblotting for sites known to be phosphorylated by MAP kinases: ATF2, pT51/53; c-Jun, S73; c-Myc, pT58/S62 (examples of primary data, Fig. S5*B*). Mean ± SE ($n = 4$ pairs). Asterisks indicate statistical significance ($P < 0.05$).

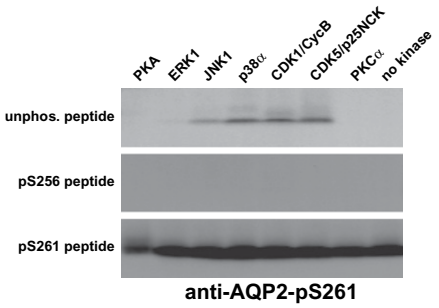

Fig. 5. Identification of kinases capable of phosphorylating AQP2 at S261. In vitro incubation (1 h at 30°C) of indicated kinases with each of three synthetic peptides corresponding to the COOH-tail of AQP2 (unphosphorylated. peptide, pS256 peptide, and pS261 peptide). Peptides phosphorylated at S261 were detected by immunoblotting with anti–AQP2-pS261 antibody.

those seen in congestive heart failure, hepatic cirrhosis, cancer-associated syndrome of inappropriate antidiuresis, and acquired forms of diabetes insipidus (12).

In this study, we have used an LC-MS/MS approach to large-scale quantification of phosphopeptides using stable isotope labeling in a mouse collecting duct cell line. These cells have been recloned to maximize the expression level of the water channel AQP2 and to select for responses to vasopressin resembling those seen in native collecting ducts (7). In the current study we identified a total of 3,869 phosphopeptides, corresponding to 1,695 phosphoproteins. Of the phosphopeptides quantified, the vast majority did not change in abundance following dDAVP treatment for 30 min (Fig. 1*C*). Among the phosphopeptides that did change, informative patterns emerged (Fig. 2). Specifically the majority of sites at which phosphorylation increased were so-called "basophilic" sites (indicating a presence of basic amino acids in key positions that determine site-specificity of phosphorylation), whereas the majority of sites that were decreased in phosphorylation were so-called "proline-directed" sites (indicating a presence of proline moieties in key positions). These patterns give important clues to the identities of the kinases involved in the phosphorylation events (18).

Basophilic S/T kinases include those in the AGC family of protein kinases that includes PKA, protein kinase C, and protein kinase G isoforms. The most frequent motif identified, R-R/K-X-S, is compatible with phosphorylation by PKA, which is regulated by cAMP. Although PKA is believed to phosphorylate AQP2 at S256, Brown et al. (20) have emphasized that several other basophilic kinases, having compatible sequence preferences, could also play a role in vasopressin-dependent phosphorylation of AQP2 at S256. In addition, calmodulin-regulated kinases, such as CaMK II, are basophilic S/T kinases. CaMK II was shown in the present study to undergo an increase in autophosphorylation (T286) in response to dDAVP in both the native tissue and mpkCCD cells (Fig. S4 *A* and *B*). Our previous study demonstrated that vasopressin also triggers another calmodulin-dependent phosphorylation event, viz. myosin light chain kinase-mediated phosphorylation of the myosin regulatory light chain protein (13), which is critical to AQP2 trafficking and is dependent on V2 receptor–dependent calcium mobilization (2, 21, 22). Of particular interest was the confirmation of increased CREB1 phosphorylation at Ser133 and the finding of increased stathmin phosphorylation at S15, both known CaM kinase II targets (15, 17). Overall, the predominance of increased phosphorylation at basophilic sites in mpkCCD proteins is consistent with current views of vasopressin signaling that both cAMP and Ca^{2+}-calmodulin are important second messengers central to the regulation of water permeability in collecting ducts.

A particularly informative observation was the predominance of proline-directed sites among the phosphorylation targets that were significantly down-regulated. Proline-directed kinases include both MAP kinases and cyclin-dependent kinases. We suspected the former because the predominant target site for our dataset, P-X-S-P, favors phosphorylation by MAP kinases (Fig. S5*B*) and because of prior studies implicating MAP kinases in vasopressin signaling (22–25). Despite the lack of agreement on whether vasopressin increases or decreases MAP kinase activities, the broad decrease in phosphorylation at sites compatible with MAP kinase targets seen in the present study supports the idea that, under normal circumstances, vasopressin decreases MAP kinase activities. Follow-up experiments in mpkCCD cells demonstrated that vasopressin decreases activation of ERK1/2 and JNK1/2 but does not alter p38 activation.

Previously, we demonstrated that vasopressin regulates phosphorylation of four serines in the COOH-terminal tail of AQP2 (26, 27). It increases phosphorylation at S256, S264 and S269, and decreases phosphorylation at S261. The presence of a proline immediately following S261 suggests that the decrease in phosphorylation at this site may be part of the broad decrease in phosphorylation of MAP kinase targets. To test whether specific MAP kinases can phosphorylate S261 of AQP2, we carried out in vitro incubations of synthetic COOH-terminal AQP2 peptides with purified MAP kinases and probed the product with a phosphospecific antibody to this site. The results demonstrate strong phosphorylation of S261 by JNK, p38, and CDK5/9 and weaker phosphorylation by ERK. Similar assays confirmed that PKA can phosphorylate S256 of AQP2 but not S261 or S264 (27). Thus, the combination of results points to a role for MAP kinases (possibly JNK) in S261 phosphorylation in mpkCCD cells.

In summary, the advent of sequence information from single species genome sequencing projects, as well as the development of more accurate and sensitive mass spectrometers, have allowed a "systems-level" approach to understanding signaling networks with the goal of comprehensively mapping and quantifying protein phosphorylation, as well as other posttranslational modifications. The results of the current study greatly expand the list of known vasopressin-regulated phosphoproteins while uncovering generalized patterns in activation and deactivation of classes of kinases, indicating that vasopressin binding to the V2R perturbs several signaling pathways.

Methods

SILAC and Cell Culture. All SILAC reagents and media were obtained from Invitrogen. An AQP2-expressing mpkCCD clonal cell line (clone 11) (7) was grown on membrane supports (Transwell, Corning. Cells were grown separately in culture medium containing the amino acids arginine and lysine labeled with stable isotopes ("heavy": $^{13}C_6{}^{15}N_4$ arginine, $^{13}C_6$ lysine; "light": $^{12}C_6{}^{14}N_4$ arginine, $^{12}C_6$ lysine) for 16 days (five passages). This labeling period is sufficient to achieve ~98% saturation of labeling (Tables S1).

Figure S6*A* shows an outline of a SILAC-based quantitative phosphoproteomic experiment. Transepithelial resistance was measured daily to ensure equal cell growth and polarization (Fig. S1*A*). Cells labeled with heavy or light amino acids were exposed to either dDAVP (0.1 nM) or vehicle (30 min) after prior withdrawal of dDAVP for 6 h. Treatment groups were varied with respect to the label. Protein lysates (2–3 mg each population) were pooled in a 1:1 ratio and subjected to phosphopeptide purification steps. Enriched phosphopeptides were analyzed on a Thermo LTQ-Orbitrap mass spectrometer (Thermo Electron) as described in *SI Text*.

Computational Analysis. A workflow for analysis of phosphorylation data is outlined in Fig. S6*B*. The MS spectra were searched using three different search algorithms: InsPecT (28), SEQUEST (29), and OMSSA (30). For MS2 spectra, the fixed modification was carbamidomethylation of cysteine, whereas the variable modifications were phosphorylation of Ser, Thr, and Tyr, isotope labeling of arginine (+ 6.02 Da) and lysine (+ 10.01 Da), and oxidation of methionine with a maximum of four modifications. For MS3 spectra, the variable modification of neutral loss of water (−18Da, for Ser and Thr) was added. A total of three missed cleavages were allowed per peptide. Searches were performed against the most recent mouse RefSeq Database using the target-decoy approach (31) with filters set to obtain <2% FDR based on identification of decoy sequences. Both OMSSA and InsPecT searches were performed on the National Institutes of Health Biowulf cluster (http://biowulf.nih.gov). Filtered peptide data have been deposited with Peptidome (National Center for Biotechnology Information, accession number PSE131). Quantification of phosphopeptides (area

under the curve of reconstructed ion chromatograms) used *QUIL*, an in-house algorithm for quantification of isotope labeled peptides by LC-MS (32).

Phosphorylation site assignment was performed using the following scoring algorithms: *Ascore* (33) and *PhosphoScore* (34) for SEQUEST data, and *Phosphate Localization Score* for InsPecT data (35). Final assignment of phosphorylation sites was performed using in-house programs (*NHLBI ProMatch* and *PhosphoPIC*).

Analysis of phosphorylation motifs was performed using the open-access *motif-x* algorithm (8) (minimal number of occurrences, 20; peptide sequences extended by six amino acids via mouse IPI proteome database; the entire mouse proteome used as background). Classification of phosphorylation motifs was also performed using a binary decision tree algorithm (9).

ACKNOWLEDGMENTS. This work was funded by the Division of Intramural Research, National Heart, Lung and Blood Institute (NHLBI; project ZO1-HL001285, M.A.K.). We thank Samuel H. Payne for advice regarding InsPecT. M.M.R. was supported by the Braun Foundation (Melsungen, Germany) and the Biomedical Sciences Exchange Program (Hannover, Germany). Mass spectrometry was performed in the NHLBI Proteomics Core Facility (director, Marjan Gucek).

1. Hoffert JD, Chou CL, Knepper MA (2009) Aquaporin-2 in the "-omics" era. *J Biol Chem* 284:14683–14687.
2. Yip KP (2002) Coupling of vasopressin-induced intracellular $Ca2^+$ mobilization and apical exocytosis in perfused rat kidney collecting duct. *J Physiol* 538:891–899.
3. Ibarrola N, Kalume DE, Gronborg M, Iwahori A, Pandey A (2003) A proteomic approach for quantitation of phosphorylation using stable isotope labeling in cell culture. *Anal Chem* 75:6043–6049.
4. Gruhler A, et al. (2005) Quantitative phosphoproteomics applied to the yeast pheromone signaling pathway. *Mol Cell Proteomics* 4:310–327.
5. Krüger M, et al. (2008) Dissection of the insulin signaling pathway via quantitative phosphoproteomics. *Proc Natl Acad Sci USA* 105:2451–2456.
6. Amanchy R, et al. (2009) Identification of c-Src tyrosine kinase substrates in platelet-derived growth factor receptor signaling. *Mol Oncol* 3:439–450.
7. Yu MJ, et al. (2009) Systems-level analysis of cell-specific AQP2 gene expression in renal collecting duct. *Proc Natl Acad Sci USA* 106:2441–2446.
8. Schwartz D, Gygi SP (2005) An iterative statistical approach to the identification of protein phosphorylation motifs from large-scale data sets. *Nat Biotechnol* 23: 1391–1398.
9. Villén J, Beausoleil SA, Gerber SA, Gygi SP (2007) Large-scale phosphorylation analysis of mouse liver. *Proc Natl Acad Sci USA* 104:1488–1493.
10. Wang Q, Margolis B (2007) Apical junctional complexes and cell polarity. *Kidney Int* 72:1448–1458.
11. Noda Y, Sasaki S (2006) Regulation of aquaporin-2 trafficking and its binding protein complex. *Biochim Biophys Acta* 1758:1117–1125.
12. Nielsen S, et al. (2002) Aquaporins in the kidney: From molecules to medicine. *Physiol Res* 82:205–244.
13. Chou CL, et al. (2004) Non-muscle myosin II and myosin light chain kinase are downstream targets for vasopressin signaling in the renal collecting duct. *J Biol Chem* 279:49026–49035.
14. Brickey DA, et al. (1994) Mutational analysis of the autoinhibitory domain of calmodulin kinase II. *J Biol Chem* 269:29047–29054.
15. le Gouvello S, Manceau V, Sobel A (1998) Serine 16 of stathmin as a cytosolic target for $Ca2^+$/calmodulin-dependent kinase II after CD2 triggering of human T lymphocytes. *J Immunol* 161:1113–1122.
16. Yasui M, Zelenin SM, Celsi G, Aperia A (1997) Adenylate cyclase-coupled vasopressin receptor activates AQP2 promoter via a dual effect on CRE and AP1 elements. *Am J Physiol* 272:F443–F450.
17. Shaywitz AJ, Greenberg ME (1999) CREB: A stimulus-induced transcription factor activated by a diverse array of extracellular signals. *Annu Rev Biochem* 68:821–861.
18. Miller ML, et al. (2008) Linear motif atlas for phosphorylation-dependent signaling. *Sci Signal* 1:ra2.
19. Davis RJ (2000) Signal transduction by the JNK group of MAP kinases. *Cell* 103: 239–252.
20. Brown D, Hasler U, Nunes P, Bouley R, Lu HA (2008) Phosphorylation events and the modulation of aquaporin 2 cell surface expression. *Curr Opin Nephrol Hypertens* 17: 491–498.
21. Chou CL, Yip KP, Knepper MA (1999) Role of Ca/calmodulin in vasopressin-stimulated aquaporin-2 trafficking in rat collecting duct. *J Am Soc Nephrol* 10:13A.
22. Pisitkun T, et al. (2008) Akt and ERK1/2 pathways are components of the vasopressin signaling network in rat native IMCD. *Am J Physiol Renal Physiol* 295:F1030–F1043.
23. Yamada T, et al. (1995) AVP inhibits EGF-stimulated MAP kinase cascade in Madin-Darby canine kidney cells. *Kidney Int* 48:745–752.
24. Umenishi F, Narikiyo T, Vandewalle A, Schrier RW (2006) cAMP regulates vasopressin-induced AQP2 expression via protein kinase A-independent pathway. *Biochim Biophys Acta* 1758:1100–1105.
25. Michlig S, et al. (2004) ERK1/2 controls Na,K-ATPase activity and transepithelial sodium transport in the principal cell of the cortical collecting duct of the mouse kidney. *J Biol Chem* 279:51002–51012.
26. Hoffert JD, Pisitkun T, Wang G, Shen RF, Knepper MA (2006) Quantitative phosphoproteomics of vasopressin-sensitive renal cells: Regulation of aquaporin-2 phosphorylation at two sites. *Proc Natl Acad Sci USA* 103:7159–7164.
27. Hoffert JD, et al. (2008) Vasopressin-stimulated increase in phosphorylation at Ser269 potentiates plasma membrane retention of aquaporin-2. *J Biol Chem* 283:24617–24627.
28. Tanner S, et al. (2005) InsPecT: Identification of posttranslationally modified peptides from tandem mass spectra. *Anal Chem* 77:4626–4639.
29. Eng JK, McCormack AL, Yates JR III (1994) An approach to correlate tandem mass spectral data of peptides with amino acid sequences in a protein database. *J Am Soc Mass Spectrom* 5:976–989.
30. Geer LY, et al. (2004) Open mass spectrometry search algorithm. *J Proteome Res* 3: 958–964.
31. Elias JE, Gygi SP (2007) Target-decoy search strategy for increased confidence in large-scale protein identifications by mass spectrometry. *Nat Methods* 4:207–214.
32. Wang G, et al. (2006) Automated quantification tool for high-throughput proteomics using stable isotope labeling and LC-MS^n. *Anal Chem* 78:5752–5761.
33. Beausoleil SA, Villén J, Gerber SA, Rush J, Gygi SP (2006) A probability-based approach for high-throughput protein phosphorylation analysis and site localization. *Nat Biotechnol* 24:1285–1292.
34. Ruttenberg BE, Pisitkun T, Knepper MA, Hoffert JD (2008) PhosphoScore: An open-source phosphorylation site assignment tool for MS^n data. *J Proteome Res* 7: 3054–3059.
35. Payne SH, et al. (2008) Phosphorylation-specific MS/MS scoring for rapid and accurate phosphoproteome analysis. *J Proteome Res* 7:3373–3381.